Applied Catalysis B: Environmental 100 (2010) 386–392

Contents lists available at ScienceDirect

Applied Catalysis B: Environmental

journal homepage: www.elsevier.com/locate/apcatb

Photocatalytic reduction of CO_2 with H_2O on mesoporous silica supported Cu/TiO_2 catalysts

Ying Li[a,b,*], Wei-Ning Wang[b], Zili Zhan[b], Myung-Heui Woo[c], Chang-Yu Wu[c], Pratim Biswas[b,1]

[a] Department of Mechanical Engineering, University of Wisconsin-Milwaukee, Milwaukee, WI 53211, USA
[b] Department of Energy, Environmental and Chemical Engineering, Washington University in St. Louis, St. Louis, MO 63130, USA
[c] Department of Environmental Engineering Sciences, University of Florida, Gainesville, FL 32611, USA

ARTICLE INFO

Article history:
Received 9 February 2010
Received in revised form 12 August 2010
Accepted 16 August 2010
Available online 21 August 2010

Keywords:
Photocatalysis
TiO_2
Nanocomposite
CO_2 photoreduction

ABSTRACT

Photoreduction of CO_2 to hydrocarbons is a sustainable energy technology which not only mitigates emissions but also provides alternative fuels. However, one of the largest challenges is to increase the overall CO_2 photo-conversion efficiency when water is used as the reducing reagent. In this work, mesoporous silica supported Cu/TiO_2 nanocomposites were synthesized through a one-pot sol–gel method, and the photoreduction experiments were carried out in a continuous-flow reactor using CO_2 and water vapor as the reactants under the irradiation of a Xe lamp. The high surface area mesoporous silica substrate (>300 m^2/g) greatly enhanced CO_2 photoreduction, possibly due to improved TiO_2 dispersion and increased adsorption of CO_2 and H_2O on the catalyst. CO was found to be the primary product of CO_2 reduction for TiO_2–SiO_2 catalysts without Cu. The addition of Cu species, which was identified to be Cu_2O by the XPS, markedly increased the overall CO_2 conversion efficiency as well as the selectivity to CH_4, by suppressing the electron–hole recombination and enhancing multi-electron reactions. A synergistic effect was observed by combining the porous SiO_2 support and the deposition of Cu on TiO_2. The peak production rates of CO and CH_4 reached 60 and 10 μmol g-cat^{-1} h^{-1}, respectively, for the 0.5%Cu/TiO_2–SiO_2 composite that has the optimum Cu concentration; the peak quantum yield was calculated to be 1.41%. Deactivation and regeneration of the catalyst was observed and the mechanism was discussed. Desorption of the reaction intermediates from the active sites may be the rate limiting step.

1. Introduction

Increasing levels of greenhouse gases in the atmosphere is the primary cause of global warming. Release of carbon dioxide (CO_2) from fossil fuel combustion is the major contributor to this phenomenon. Recently, many efforts are made to reduce CO_2 emissions through pre- or post-combustion CO_2 capture followed by compression and geological sequestration [1]. These processes are energy intensive and thus costly; in addition, there are many uncertainties with regard to long-term storage of CO_2 in geological formations. An alternative and more preferable way is to recycle CO_2 as a fuel feedstock with energy input from cheap and abundant sources (e.g. solar energy).

Recent innovations in photocatalysis technology have made CO_2 conversion a potentially promising application. This process utilizes ultraviolet (UV) and/or visible light as the excitation source for semiconductor catalysts, and the photoexcited electrons reduce CO_2 with H_2O on the catalyst surface and form energy-bearing products such as carbon monoxide (CO), methane (CH_4), methanol (CH_3OH), formaldehyde (HCHO), and formic acid (HCOOH) [2]. A variety of photocatalysts such as TiO_2, CdS, ZrO_2, ZnO, and MgO have been studied, and among them, wide band-gap TiO_2 catalysts (~3.2 eV) are considered the most convenient candidates in terms of cost and stability [2–4]. To enhance reaction rate, increase solar utilization, and control the selectivity of products are the major challenges so far in CO_2 photoreduction technology.

An increased CO_2 conversion efficiency was observed when the TiO_2 surface was loaded with metals, which function as "charge-carrier traps" and suppress recombination of photoexcited electron–hole pairs. Metals can be deposited on TiO_2 surface via methods of incipient wetness impregnation [5], sol–gel [6], photoreduction [7], and sputter coating [8], etc. Tseng et al. [6] used sol–gel derived Cu/TiO_2 catalysts for CO_2 photoreduction in aqueous phase and found the yield of methanol is much higher than those without Cu loading. Yamashita et al. [5] reported formation of CH_4 by TiO_2 photocatalysts in a CO_2 and H_2O system, and Cu impregnated on TiO_2 resulted in additional formation of

* Corresponding author at: Department of Mechanical Engineering, University of Wisconsin-Milwaukee, Milwaukee, WI 53211 USA. Tel.: +1 414 229 3716, fax: +1 414 229 6958.
E-mail addresses: liying@uwm.edu (Y. Li), pratim.biswas@wustl.edu (P. Biswas).
[1] Tel: +1 314 935 5548; fax: +1 314 935 5464.

0926-3373/$ – see front matter © 2010 Elsevier B.V. All rights reserved.
doi:10.1016/j.apcatb.2010.08.015

CH_3OH. Another research by Ishitani et al. [9] reported that CO_2 photoreduction using Pd, Rh, Pt, Au, Cu, and Ru deposited on TiO_2 photocatalyst produces CH_4 and acetic acid, with Pd/TiO_2 exhibiting high selectivity for CH_4 production. Varghese et al. [8] reached high-rate solar photocatalytic conversion of CO_2 and H_2O to hydrocarbons by using N-doped TiO_2 nanotubes with Pt and/or Cu as co-catalysts. Other studies investigated incorporation of Ti species in silica-based micro/mesoporous materials to enhance photocatalytic reduction of CO_2. Anpo et al. [10] and Yamashita et al. [11] reported that highly dispersed tetrahedrally coordinated TiO_2 species incorporated in mesoporous silica matrix of MCM-41 and MCM-48 showed higher reactivity and selectivity for the formation of CH_3OH compared to small TiO_2 particles. Ikeue et al. [12] and Shioya et al. [13] synthesized Ti-containing porous silica thin film for CO_2 photoreduction with a quantum yield of 0.28% at 323 K for CH_3OH production, which is remarkably higher than powdered Ti-MCM-41 catalyst (quantum yield was 0.02%). The high yield and selectivity can be attributed to their high transparency and large amount of surface OH species on the catalysts.

Since both strategies (surface deposition of metals on TiO_2 and porous silica as the support for TiO_2) can enhance photoreduction of CO_2, it is important to study the synergistic effect of both metal addition and silica support on the photocatalytic activity of TiO_2 catalysts. Sasirekha et al. [14] prepared Ru doped anatase supported on silica particles and found $Ru–TiO_2/SiO_2$ was more active than Ru/TiO_2 for methanol production but there was no enhancement compared to TiO_2/SiO_2. While doping of noble metals is costly, the addition of copper, a cheap co-catalyst to TiO_2 warrants future investigation. In addition, mesoporous silica is superior to silica particles as a catalyst support due to its much higher surface area. To the best of our knowledge, no research has been reported on the synthesis of Cu loaded TiO_2 catalysts supported on mesoporous silica and their activity toward photocatalytic CO_2 reduction. In this work, we used a one-pot sol–gel method for synthesis of $Cu/TiO_2–SiO_2$ catalysts. Because of the low solubility of CO_2 in water, the photocatalysis was performed in a gas–solid interface in this study. In addition, the reactor design is different from most of those reported in the literature, where batch reactors were used and reaction equilibrium was typically reached after a certain amount of time (usually in the order of hours) and formation of the reaction products ceased. In other words, batch reactors are not suitable for long-term testing of catalyst performance. Furthermore, continuous-flow reactors are more appropriate than batch reactors from a practical point of view, because larger scale applications require continuous collection of reaction products. Therefore, a continuous-flow photoreactor was designed in this study to test the activity of synthesized $Cu/TiO_2–SiO_2$ catalysts on CO_2 reduction. The role of Cu species and concentrations as well as the effect of silica support on the catalytic activity were also investigated.

2. Experimental

2.1. Catalyst preparation

In this work, a one-pot sol–gel method was used to synthesize the porous SiO_2 supported Cu/TiO_2 catalysts. To compare the catalytic activities, SiO_2 supported TiO_2 catalysts without Cu loading were also prepared following the procedure described in our previous work [15,16]. In a typical preparation process, 25 mL deionized (DI) water, 50 mL ethanol, and 35 mL tetraethyl orthosilicate (TEOS) were first added to a polymethylpentene container with vigorous magnetic stirring. Then 4 mL 1 M HNO_3 and 4 mL 3% HF were added as catalysts to increase the hydrolysis and condensation rates. Meanwhile, a certain amount (1.0 g in this work) of Degussa P25 TiO_2 nanoparticles was added to the batch. To incorporate Cu species into the matrix, a measured amount of $CuCl_2$ was dissolved in the 25 mL DI water added in the beginning. After approximately 2 h, the sol suspended with TiO_2 nanoparticles was pipetted into polystyrene 96-well assay plates before the gelation occurred. The pellets were later aged at room temperature for 2 days and then at 65 °C for another 2 days. After aging, the pellets were removed from the plates and thoroughly rinsed with DI water to remove any residual acid or ethanol. Next, the pellets were placed in a programmable oven and heated at 103 °C for 18 h to remove any residues of liquid solution within the silica network and then at 180 °C for 6 h to harden the gel. Finally the temperature was slowly decreased back to room temperature over a 90 min period. The synthesized pellets were cylindrical approximately 5 mm in length and 3 mm in diameter. The pellets were finally ground to powders and sieved through a #150 mesh (100 μm opening). In this work, the concentration of TiO_2 in the composite was maintained at 12 wt%, which corresponded to the optimum performance on photocatalytic oxidation of elemental mercury by the $TiO_2–SiO_2$ catalysts [15,16]. The Cu loading on the $Cu/TiO_2–SiO_2$ catalysts varied from 0.2 to 3 wt%, or 1.7 to 25 wt% relative to TiO_2, which was calculated from the amount of $CuCl_2$ added.

The powder catalyst (<100 μm) of $Cu/TiO_2–SiO_2$ was loaded as a thick film on a glass fiber filter when used in the photocatalytic reaction. It was prepared as follows: a select amount of $Cu/TiO_2–SiO_2$ powder was first dispersed in ethanol and then evenly dipped on a glass fiber filter, followed by drying at 80 °C for 3 h and subsequently at 180 °C for 30 min. To investigate the effect of porous SiO_2 support, Cu/TiO_2 catalyst without SiO_2 support was prepared by mixing P25 TiO_2 nanoparticles and $CuCl_2$ in ethanol, sonicating in ultrasonic bath for 5 min, dipping the mixture evenly on glass fiber filter, and following the same drying process as described above. TiO_2 catalyst without Cu was also prepared by loading only P25 nanoparticles on a glass fiber filter. The amount of catalyst powders used was 100 mg for all cases.

2.2. Catalyst characterization

The BET surface areas of the powder catalysts were measured using a Quantachrome Autosorb-1 surface area and pore size analyzer (Boynton Beach, FL). X-ray diffraction (XRD) patterns of the powders were recorded with a Philips APD 3720 diffractometer using Cu-Kα radiation ($\lambda = 0.1542$ nm) in the range of 20–50° (2θ) with a step size of 0.02°. X-ray photoelectron spectroscopy (XPS) analysis of the samples was carried out by a Perkin-Elmer PHI 5100 ESCA system using Mg Kα ($h\nu = 1253.6$ eV) radiation to excite photoelectrons. A diffuse reflectance UV–vis spectrophotometer (Varian, Cary 100) was used to obtain the UV–vis spectra of the catalysts. The inner structure of the catalyst was analyzed by transmission electron microscopy (TEM) (JEM-2100F, JEOL, Tokyo, Japan). Before TEM analysis, the as-prepared nanocomposites were dried in a vacuum oven for 24 h to eliminate any organic residues inside the mesoporous structure, which were then suspended in ethanol and followed by sonication for 30 min prior to dispersion onto a TEM grid with a lacey support film.

2.3. Photocatalytic reaction

A continuous-flow reactor system was designed for photocatalytic reaction as shown in Fig. 1. Compressed CO_2 (99.99%, Cee Kay Suppy, Inc.), controlled by a mass flow controller, was passed through a water bubbler to generate a mixture of CO_2 and water vapor. The reactant gas was then introduced to the cylindrical continuous-flow reactor, which was built with a stainless steel

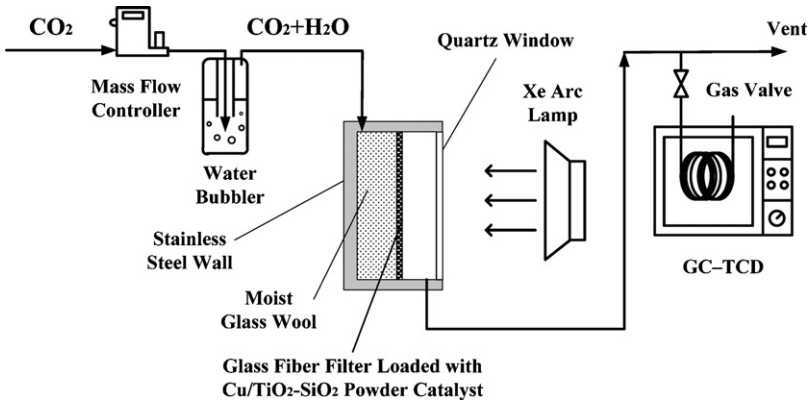

Fig. 1. Schematic of experimental setup for photoreduction of CO_2 with H_2O.

wall and a quartz window at the top. The inner cavity was 6.0 cm in diameter and 2.5 cm deep. Glass wool was placed in the reactor as the support for the glass fiber filter loaded with a thick film of powder catalysts. The glass wool support was also moisturized with 3.0 g DI water to maintain saturated water vapor in the reactor. A Xe arc source system (Newport, Model 63220) was the irradiation source and a liquid cooler was mounted to absorb the infrared portion of the light. As shown in Fig. 2, the light intensity of the lamp at the location of catalyst was 2.4 mW/cm^2 for 250 nm < λ < 400 nm measured by a spectroradiometer (Polytec, ILT-900R), and its intensity was less than solar irradiation (AM 1.5G standard) for λ < 650 nm. The concentrations of effluent gases (e.g. CO, CH_4, and CO_2) from the reactor were continuously measured by a gas-chromatography (GC) through an automated gas valve, using helium as the carrier gas. The GC was equipped with a 30 m × 0.32 mm PLOT capillary column (Supelco Carboxen-1010) and a thermal conductivity detector (TCD). Since this study focused on CO_2 reduction on gas–solid interface, possible products such as methanol, formaldehyde, and formic acid were not measured which are more likely produced in CO_2 photoreduction in aqueous solutions [6,14,17,18]. Before each test, the reactor loaded with catalyst was first purged with the $CO_2 + H_2O$ mixture at 100 mL/min for 45 min and then the flow rate was reduced and maintained at 3.0 mL/min. After 30 min when the flow was stabilized, the Xe lamp was turned on and the concentrations of effluent gases as a function of irradiation time were recorded.

Table 1
BET specific surface area of the silica supported catalysts.

Catalyst*	Specific surface area (m^2/g)
TiO_2–SiO_2	355.5
0.5%Cu/TiO_2–SiO_2	386.2
1%Cu/TiO_2–SiO_2	385.6
3%Cu/TiO_2–SiO_2	371.8

* TiO_2 weight concentration is 12% for all catalysts.

3. Results and discussion

3.1. Characteristics of catalysts

Table 1 lists the BET specific surface area (SSA) of the catalysts. The TiO_2–SiO_2 catalyst had a high surface area of 355.5 m^2/g. The addition of Cu species to the TiO_2–SiO_2 slightly increased the SSA, with 0.5% and 1% Cu corresponding to the highest SSA (~386 m^2/g). It was reported by Nguyen and Wu [19] that the addition of 0.5% Cu and 0.5% Fe to TiO_2–SiO_2 thin film dramatically decreased the SSA. Hence, the synthesis method used in this work is advantageous in terms of preserving the high surface area of the catalysts.

Fig. 3 shows the XRD patterns of the Cu/TiO_2–SiO_2 catalysts with Cu loading from 0% to 3%. All patterns clearly show both anatase and rutile phases of TiO_2, which agrees with the composition of Degussa P25 (approximately 80% anatase and 20% rutile). The result

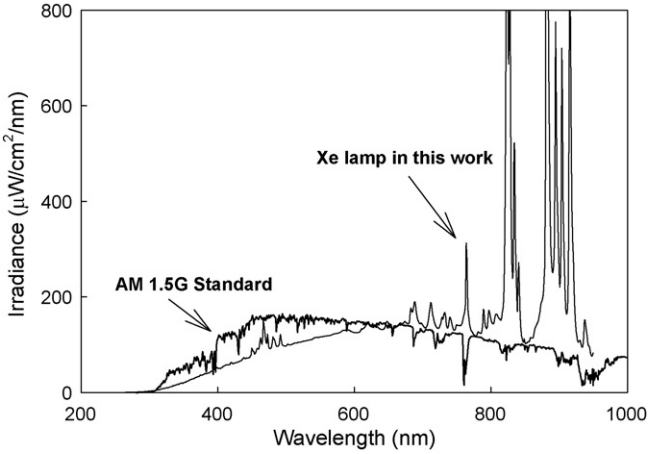

Fig. 2. Irradiance spectrum of sunlight (AM 1.5G standard) and Xe lamp used in this work.

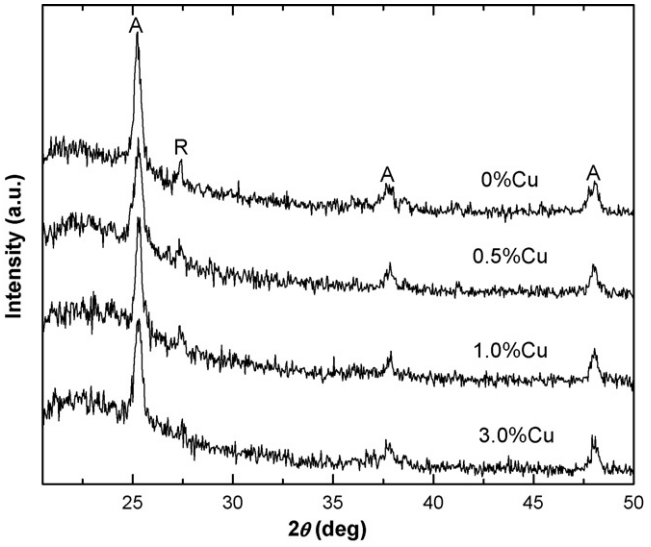

Fig. 3. XRD patterns of Cu/TiO_2–SiO_2 catalysts at various Cu loading (A = Anatase; R = Rutile).

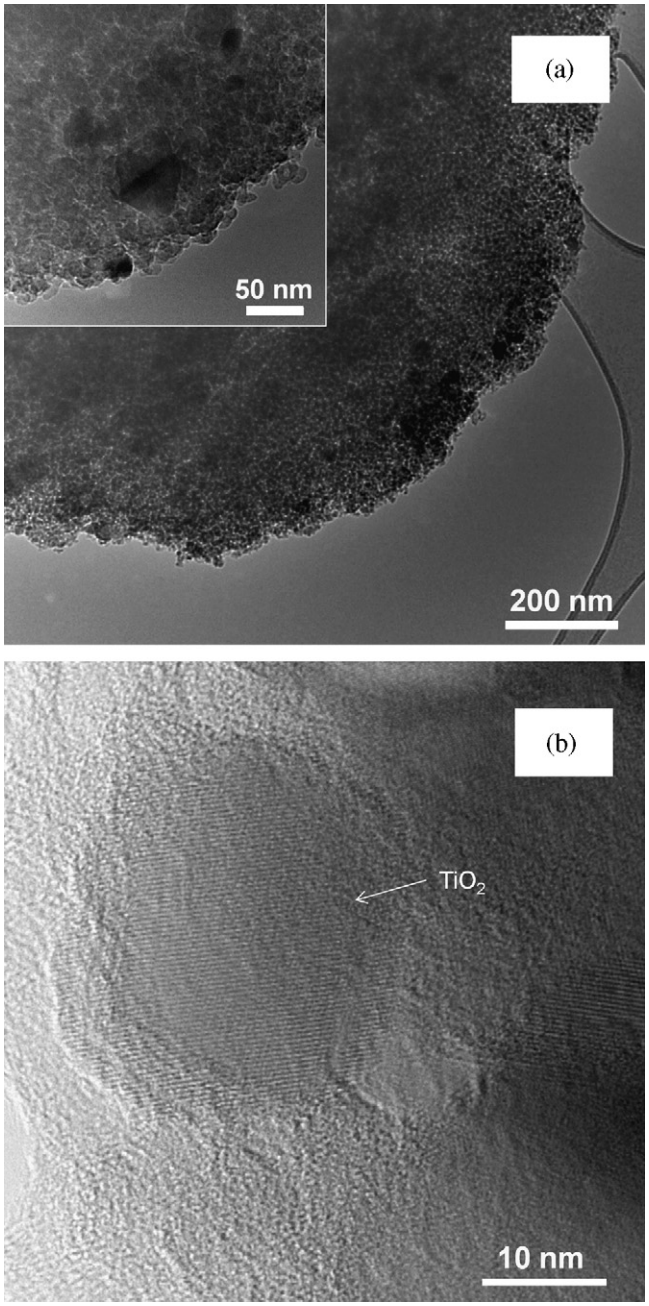

Fig. 4. TEM image of 0.5%Cu/TiO_2–SiO_2 nanocomposite (a) and HR-TEM image of a single TiO_2 nanocrystal (b).

indicates that the catalyst preparation process did not affect the phase of TiO_2 nanoparticles. Diffraction peaks for copper species were not detected, indicating Cu is highly dispersed [20,21] or due to the low Cu concentration and extremely small Cu clusters [6]. It also shows that the deposition of Cu did not affect the crystalline structure of TiO_2.

The TEM and high resolution TEM (HR-TEM) images of the 0.5%Cu/TiO_2–SiO_2 nanocomposite are shown in Fig. 4. A homogeneous mesoporous structure of SiO_2 is clearly observed. The irregular-shaped dark particles embedded in the SiO_2 framework are P25 TiO_2 nanoparticles, which have an average size around 20 nm. However, the dispersion of TiO_2 nanoparticles is not uniform. The HR-TEM image shows clear lattice fringes of TiO_2 nanoparticles and confirms the crystallinity of the P25 TiO_2. It also verifies the amorphous structure of the SiO_2 support. Due to the extremely low concentration of Cu, no individual Cu particles were observed from the images.

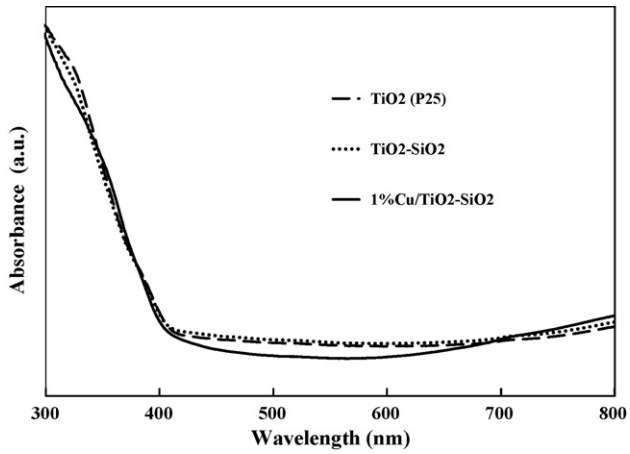

Fig. 5. UV–vis spectra of various TiO_2-containing catalysts.

The UV–vis absorption spectra of the catalysts are shown in Fig. 5. The catalysts absorb light below 400 nm, corresponding to a band-gap approximately 3.1 eV. There was no significant difference between the spectra of TiO_2, TiO_2–SiO_2, and 1%Cu/TiO_2–SiO_2, indicating the low concentration of Cu did not shift the absorption spectrum of TiO_2.

The Cu 2p XPS spectrum of 10%Cu/TiO_2–SiO_2 catalyst is shown in Fig. 6. It should be noted that no Cu peaks were observed in the XPS with 1% or 3% Cu loading, probably due to the low Cu concentration on the surface. With 10% Cu loading, the binding energy of Cu $2p_{3/2}$ peak around 932.8 eV and the lack of shake-up satellite peak around 942 eV indicate characteristics of Cu_2O [5,20,22]. CuO binding energy (933–934 eV) is normally shifted by 1.3 eV above the Cu_2O peak together with shake-up satellite peaks (~942 eV) for CuO [6,22]. Hence, in this work the primary Cu species on the Cu/TiO_2–SiO_2 catalyst surface is Cu_2O.

3.2. Photoreduction of CO_2

With a mixture of CO_2 and H_2O vapor passing through the reactor, a series of background tests were first performed for the following cases: (1) empty reactor, (2) blank glass fiber filter in the reactor, (3) glass fiber filter loaded with SiO_2 only, and (4) glass fiber filter loaded with Cu ions only. No CO_2 conversion products (CO or CH_4) were observed for these cases no matter the light was on or off,

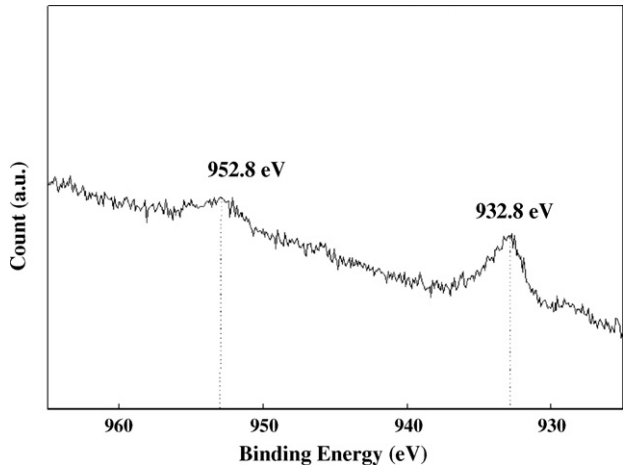

Fig. 6. Cu 2p XPS spectrum of 10%Cu/TiO_2–SiO_2 nanocomposite.

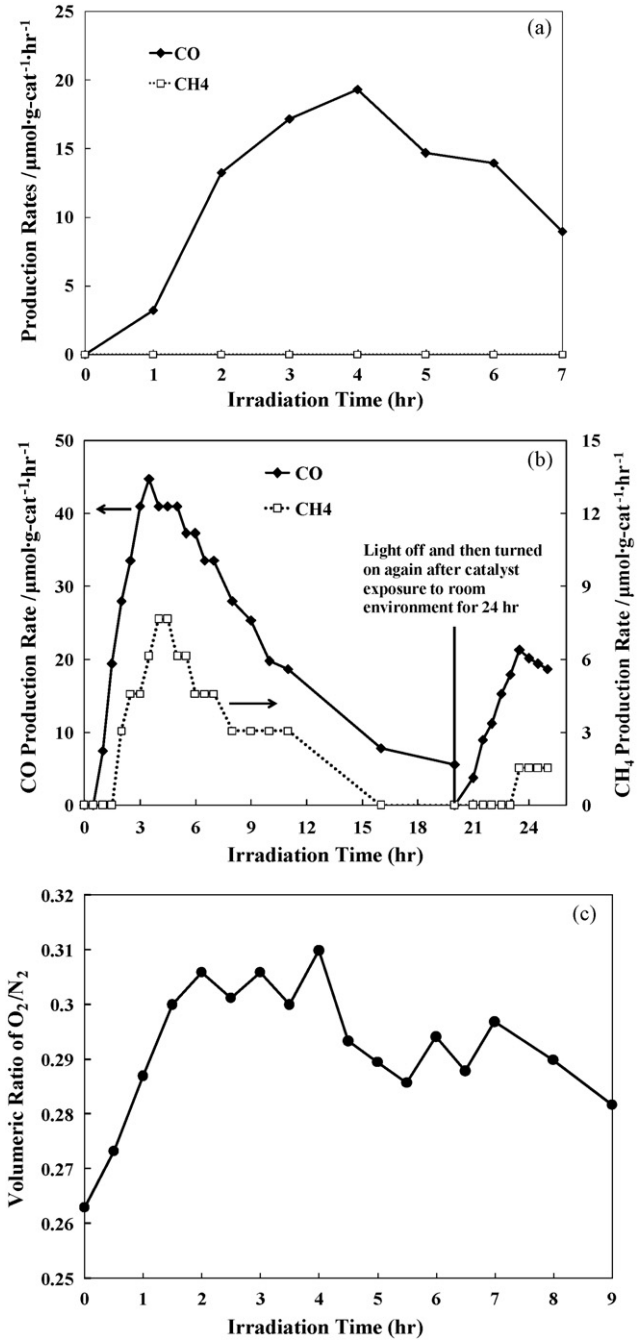

Fig. 7. Time dependence on the production rates of CO and CH_4 over TiO_2–SiO_2 (a) and 0.5%Cu/TiO_2–SiO_2 (b) and time dependence on the ratio of O_2/N_2 in the effluent gas with 0.5%Cu/TiO_2–SiO_2 as the catalyst (c).

and the conversion only occurred when TiO_2 was present together with UV irradiation. This demonstrates that the conversion products were not formed due to photo-decomposition of residue organics in the catalyst, if any, by the UV light alone. Furthermore, it confirms that this conversion is a photocatalytic reduction process that requires both TiO_2-based catalysts and UV irradiation. Additional background tests were also performed using a mixture of pure N_2 and H_2O vapor as the feed gas with Cu/TiO_2–SiO_2 catalysts in the reactor under UV irradiation, and again, no formation of carbon-containing products were observed. This verifies that the photoreduction products (e.g., CO and CH_4) were derived from CO_2 in the feed gas, not from residue organics in the catalyst, if there is any. Fig. 7 shows the production rates (in unit of μmol g-TiO_2^{-1} h^{-1}) of CO and CH_4 as a function of irradiation time for CO_2 photoreduction. Since the mass of Cu was very small compared to that of TiO_2, it is reasonable to normalize the production rates based on the mass of TiO_2 only. The calculated production rates were proportional to the concentration of products in the reactor that were continuously measured by the GC.

CO was identified as the major product using TiO_2–SiO_2 catalyst (Fig. 7a), and the CO_2 photoreduction pathway can be described as reactions (E1–E3).

$$TiO_2 \xrightarrow{h\nu} e^-_{cb}(TiO_2) + h^+_{vb}(TiO_2) \quad \text{(E1)}$$

$$2H_2O + 4h^+ \rightarrow 4H^+ + O_2 \quad \text{(E2)}$$

$$CO_2 + 2H^+ + 2e^- \rightarrow CO + H_2O \quad \text{(E3)}$$

where the conduction band (CB) flatband potential of TiO_2 (P25) is −0.56 V vs. NHE at pH 7 [23], and the reduction potential of (E3) is −0.53 V vs. NHE at pH 7 [24]. As the CB flatband potential is more negative than the CO_2/CO reduction potential, reaction (E3) is theoretically feasible. As shown in Fig. 7a, the measured production rate of CO increased with irradiation time and reached a peak value at around 4 h. Since a continuous-flow reactor was used and because the reactor volume was much larger (30 times larger) than the gas flow rate, it took time (4 h in this case) for CO concentration (or measured production rate) to reach a maximum value (19.4 μmol g-TiO_2^{-1} h^{-1}) in the reactor. However, the CO production rate did not remain steady after 4 h; rather, it gradually decreased. Similar results were reported in the study of Sasirekha et al. [14] that the yields of CO_2 photoreduction products decreased after they reached the maximum values around 6 h of UV irradiation. The reason may be attributed to the deterioration of photocatalytic activity due to diminishment of the adsorption power of the particles and saturation of the adsorption sites on the TiO_2 surface with intermediate products [14].

When 0.5% Cu species was added to the TiO_2–SiO_2 catalyst, both CO and CH_4 were detected as the reduction products (as shown in Fig. 7b). The production of CH_4 may proceed as follows:

$$CO_2 + 8H^+ + 8e^- \rightarrow CH_4 + 2H_2O \quad \text{(E4)}$$

where the reduction potential is $E^0 = -0.24$ V vs. NHE at pH 7 [24]. Although the reduction potential of (E4) is less negative than that of (E3), it requires eight electrons for (E4) to proceed, compared to two electrons for (E3). Thus, it is reasonable that the CH_4 production rate is always smaller than that of the CO. The increased selectivity of CH_4 production with the presence of Cu species can be explained as Cu species acting as electron traps and resulting in an increased probability of multi-electron reactions (e.g., eight electrons for CH_4 production).

The curves of CO and CH_4 production rate followed a similar pattern as previously described. It increased with irradiation time and reached a peak value at around 4 h. The peak production rate of CO was 45 μmol g-TiO_2^{-1} h^{-1}, more than twice as high as that without Cu addition. The peak production rate of CH_4 reached 13.2 μmol g-TiO_2^{-1} h^{-1}. After 4 h, both CO and CH_4 production rates started to drop, and CO production decreased to 5.6 μmol g-TiO_2^{-1} h^{-1} at 20 h while CH_4 production ceased at 16 h. After 20 h irradiation, the light was turned off and the photoreduction completely stopped (not shown in Fig. 7b). Then the glass fiber filter loaded with Cu/TiO_2–SiO_2 catalyst was taken out of the reactor. After sitting under room condition exposed to air for 24 h without any other particular treatment, the used catalyst was again put in the reactor and continued with the photocatalysis experiment (as shown in right part of Fig. 7b). The production of both CO and CH_4 was again observed but lower than that of the fresh catalyst. The production reached maximum at 3.5 h irradiation and gradually dropped after that. The result implies that the used catalyst was partially regen-

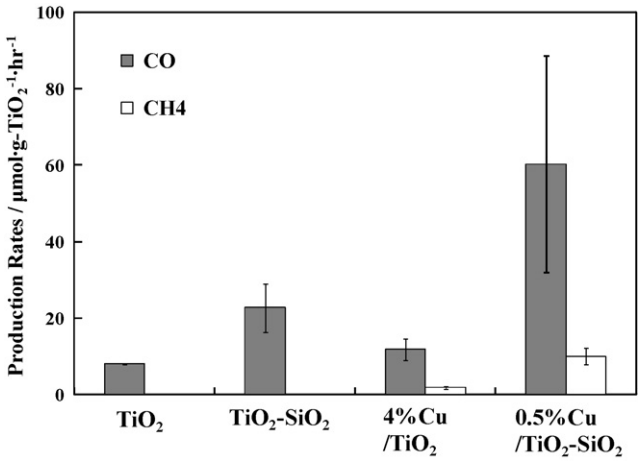

Fig. 8. Peak production rates of CO and CH_4 on various TiO_2-containing catalysts.

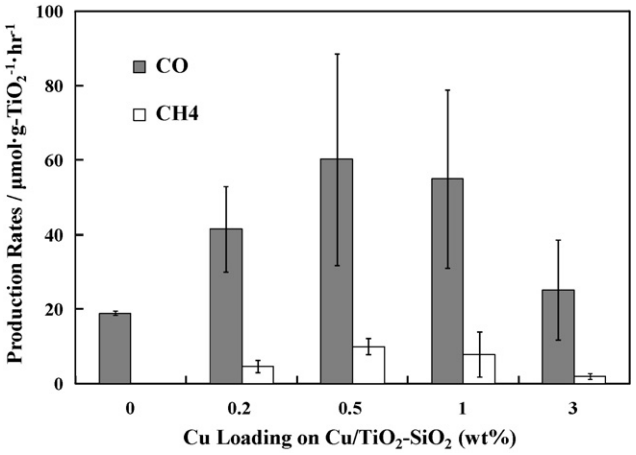

Fig. 9. Peak production rates of CO and CH_4 as a function of Cu concentration on the Cu/TiO_2–SiO_2 catalysts.

erated after sitting under room conditions. The regeneration effect may be due to desorption of the reaction products from the TiO_2 surface [25].

The concentrations of O_2 and N_2 in the effluent gas were also monitored for the above experiment using $0.5\%Cu/TiO_2$–SiO_2 as the catalyst. There was background O_2 detected in the reactor effluent gas (300–400 ppm) at the beginning of the test, possibly because the reactor was not vacuumed before purging it with the CO_2–H_2O mixture and because of the low concentration impurity gases in the CO_2 cylinder. Hence, a better indicator of O_2 production from the photocatalytic reaction is the volumetric ratio of O_2/N_2 in the effluent gas. As shown in Fig. 7c, the O_2/N_2 ratio gradually increased with the irradiation time, reached a maximum value during 2–4 h, and then decreased slowly thereafter. The time dependence of the O_2/N_2 ratio (Fig. 7c) well correlated with those of CO and CH_4 production (Fig. 7b), which implies the production of O_2 from the dissociation of H_2O according to reaction (E2). This provides another evidence of photocatalytic reaction of CO_2 and H_2O to form CO, CH_4, and O_2.

To investigate whether there is synergy of combining Cu deposition and porous SiO_2 support, four types of catalysts were compared with respect to their catalytic activities: TiO_2, $4\%Cu/TiO_2$, TiO_2–SiO_2, and $0.5\%Cu/TiO_2$–SiO_2, as shown in Fig. 8. It was designed so that the absolute mass of TiO_2 was the same (12 mg) for all the four catalysts and the mass of Cu was the same (0.5 mg) for $4\%Cu/TiO_2$ and $0.5\%Cu/TiO_2$–SiO_2 catalysts. The production rates reported in this figure were peak values as seen in Fig. 8. For each type of catalyst, experiments were carried out for three times using fresh catalysts, and the peak production rates were averaged and standard deviations reported. TiO_2 showed the lowest production rate among the four catalysts, with 8.1 μmol g-TiO_2^{-1} h^{-1} for CO and zero for CH_4. With the mesoporous SiO_2 support, CO production was enhanced to 22.7 μmol g-TiO_2^{-1} h^{-1} for TiO_2–SiO_2 but CH_4 production was still zero. The improvement may be due to the enhanced dispersion of TiO_2 and improved adsorption of CO_2 and H_2O on the high surface area SiO_2 substrate. With the addition of Cu to TiO_2, the $4\%Cu/TiO_2$ catalyst demonstrated a slightly higher CO production rate (11.8 μmol g-TiO_2^{-1} h^{-1}) than that of TiO_2, and CH_4 production occurred at a rate of 1.8 μmol g-TiO_2^{-1} h^{-1}. The above results agree with the literature that either mesoporous SiO_2 structure [10,11] or Cu loading [5,6] can enhance the photoreduction of CO_2 by TiO_2. With the combination of porous SiO_2 substrate and Cu deposition, the CO_2 photoreduction rate was significantly enhanced. For the $0.5\%Cu/TiO_2$–SiO_2 catalyst, the average peak production rates of CO and CH_4 reached 60 and 10 μmol g-TiO_2^{-1} h^{-1}, respectively. It should be emphasized that there is truly a synergistic effect due to the combination of SiO_2 substrate and Cu deposition. Taking the rate of CO production as an example, it is 8.1 μmol g-TiO_2^{-1} h^{-1} for pure TiO_2, which is enhanced by a factor of 2.8 for TiO_2–SiO_2, a factor of 1.5 for Cu/TiO_2, and a factor of 7.4 for Cu/TiO_2–SiO_2. The enhancement factor for Cu/TiO_2–SiO_2 is larger than either the sum or the product of the enhancement factors for the TiO_2–SiO_2 and Cu/TiO_2. This synergistic combination is an important finding that suggests a direction of future studies on manufacturing multi-component nanostructured catalysts for efficient CO_2 reduction.

Quantum yield of the CO_2 photo-conversion can be calculated by the following equations when CO and CH_4 are the conversion products. Two and eight electrons are required to convert CO_2 to CO and CH_4, respectively.

$$\Phi_{CO}(\%) = \frac{2 \text{ mol of CO yield}}{\text{moles of photon absorbed by catalyst}} \times 100\% \quad (1)$$

$$\Phi_{CH_4}(\%) = \frac{8 \text{ mol of } CH_4 \text{ yield}}{\text{moles of photon absorbed by catalyst}} \times 100\% \quad (2)$$

The quantum yield based on the average peak production rates was calculated to be 0.85% and 0.56% for CO and CH_4, respectively, and the total quantum yield was 1.41% for CO_2 photoreduction.

The effect of Cu concentration on the catalytic activity of Cu/TiO_2–SiO_2 was also investigated by varying the Cu loading from 0.2% to 3%. At each Cu loading level, the experiments were conducted three times, and the average peak values of production rates as well as the standard variations are shown in Fig. 9. It is clearly seen that 0.5%Cu had the highest production rates for both CO and CH_4. The production rates for 1%Cu were slightly lower than those of 0.5%Cu. Decreasing the Cu loading to 0.2% or increasing it to 3% reduced the production rates. The result agrees with the literature that there is an optimum Cu loading for CO_2 photoreduction on TiO_2-based catalysts [5,6,21,26]. At lower Cu loadings below the optimum value, Cu species can inhibit recombination of photoinduced electrons and holes by capturing the electrons, and the catalytic activity increases with Cu concentration [6,26]. However, an excess Cu loading greater than the optimum value could reduce the catalytic activity due to the possible reasons that a high concentration of Cu could mask the illuminated TiO_2 surface [6] and that excess Cu species could become recombination centers for photoinduced electrons and holes [21,26].

3.3. Discussion on photocatalytic activity

It has been reported that Cu(I) species is the active site on Cu deposited TiO_2 catalysts for photoreduction of CO_2 [5,17,20]

or photooxidation of organic compounds [7,22]. This is in agreement with the results observed in this study that Cu_2O was the primary Cu species in the fresh Cu/TiO_2–SiO_2 nanocomposites and enhanced CO_2 photoreduction efficiency. It is believed that Cu_2O on the surface of TiO_2 can trap electrons from the TiO_2 conduction band, and the trapped electrons are subsequently transferred to the surrounding adsorbed species, thereby avoiding electron–hole recombination and enhancing the photocatalytic activity. When the surface adsorbed species is primarily CO_2, the electrons will reduce CO_2, as observed in this work and in other studies.

When O_2 is also present as the surface adsorbed species, O_2 will compete with CO_2 as electron acceptors, mitigating the CO_2 reduction efficiency. The reaction can be expressed as:

$$O_2 + e^- \rightarrow O_2^- \quad \text{(E5)}$$

where the reduction potential is $E^0 = -0.28$ V vs. NHE at pH 7 [27]. The electron scavenging effect by O_2 is supported by the experimental results in this work that no CO_2 photoreduction product was observed when the reactor influent gas was changed to a mixture of O_2/CO_2 (1:1 v/v) upstream of the water bubbler. The result implies that CO_2 photoreduction is not favorable at O_2 rich environment (e.g. for atmospheric CO_2 reduction). Rather, the technology is more appropriate for CO_2 mitigation from combustion exhausts where O_2 concentration is normally less than a few percent or even close to zero in the case of oxy-fuel combustion.

An intriguing phenomenon observed in this study was the color change of the Cu-containing catalysts before and after the photocatalytic reaction, which was sparsely discussed in the literature. The fresh Cu/TiO_2–SiO_2 catalyst was almost white with very light greenish color due to the small concentration of Cu species. After a few hours CO_2 photoreduction experiment, the color of the catalyst turned to dark gray observed from the quartz window of the reactor. Interestingly, the dark color quickly turned lighter when the used catalyst was taken out of the reactor and exposed to room environment, and the color of the used catalyst almost returned to white overnight. Considering the XPS analysis result that Cu_2O was the primary Cu species for the fresh catalyst, it is very likely that the change of color to dark gray was due to the reduction of Cu(I) to Cu(0) by photoinduced electrons in the reducing environment in the photoreactor. The change of color back to white after sitting in the room condition is possibly because of the re-oxidation of Cu(0) to Cu(I) by atmospheric oxygen. Because of the fast color changing characteristics, post-reaction XPS analysis on the used catalyst was not performed. However, the above hypothesis was further validated by the following additional experimental results. First, no color change was observed for the case of TiO_2 only, confirming the color change was derived from Cu species. Second, when the experiment was conducted in O_2 rich (oxidizing) environment (1:1 ratio of O_2:CO_2), no color change of the catalyst occurred. Third, the dark color observed in the photoreduction matched the color when the catalyst was separately subject to H_2 reduction test (5% H_2 in N_2 for 2 h at 200 mL/min at 400 °C). In addition, it was reported by Tseng et al. [17] that after the H_2 reduction treatment the catalytic activity of Cu/TiO_2 was decreased for photoreduction of CO_2 to methanol, i.e. the activity of Cu(0) was inferior to that of Cu(I). Result of this work also indicated that the catalytic activity decreased together with the color change to dark [Cu(I) reduction to Cu(0)], and the activity was partially regenerated when the color returned back to white [partially re-oxidation of Cu(0) to Cu(I)]. Although the deactivation can also be contributed by other reasons such as the surface saturation with intermediate reaction products (as evidenced by the deactivation of TiO_2–SiO_2 catalyst without Cu species, Fig. 7a), it is important to stabilize the Cu_2O species at the catalyst surface to maintain the long-term performance of the Cu/TiO_2–SiO_2 catalyst. Further studies are needed in this research topic.

4. Conclusions

A simple one-pot sol–gel method was used to synthesize mesoporous silica supported Cu/TiO_2 nanocomposites. This significantly enhanced CO_2 photoreduction rates due to the synergistic combination of Cu deposition and high surface area SiO_2 support. CO and CH_4 were found to be the major gaseous products using CO_2 and H_2O vapor as the reactants for CO_2 photoreduction over Cu/TiO_2–SiO_2 catalysts. CH_4 was selectively produced when Cu species was deposited on TiO_2. The optimal Cu loading on the Cu/TiO_2–SiO_2 composite was found to be 0.5 wt%. The peak production rates of CO and CH_4 in the continuous-flow reactor and the peak quantum yield were much higher than the average values reported in the literature. Cu_2O was identified to be the active sites of electron traps, suppressing electron–hole recombination and enhancing multi-electron reactions. Cu(I) species may be reduced to Cu(0) during the photoreduction, and the Cu(0) species can be re-oxidized back to Cu(I) in air environment. The redox cycle of Cu species as well as the adsorption/desorption of reaction products on the catalysts may explain the deactivation/regeneration of the catalysts observed in this work.

Acknowledgement

The work was partially supported by a grant from the Consortium for Clean Coal Utilization.

References

[1] C.M. White, B.R. Strazisar, E.J. Granite, J.S. Hoffman, H.W. Pennline, J. Air Waste Manage. Assoc. 53 (2003) 645–715.
[2] K. Koci, L. Obalova, Z. Lacny, Chemical Papers 62 (2008) 1–9.
[3] M. Kitano, M. Matsuoka, M. Ueshima, M. Anpo, Appl. Catal. A-Gen. 325 (2007) 1–14.
[4] P. Usubharatana, D. McMartin, A. Veawab, P. Tontiwachwuthikul, Ind. Eng. Chem. Res. 45 (2006) 2558–2568.
[5] H. Yamashita, H. Nishiguchi, N. Kamada, M. Anpo, Y. Teraoka, H. Hatano, S. Ehara, K. Kikui, L. Palmisano, A. Sclafani, M. Schiavello, M.A. Fox, Res. Chem. Intermed. 20 (1994) 815–823.
[6] I.H. Tseng, W.C. Chang, J.C.S. Wu, Appl. Catal. B-Environ. 37 (2002) 37–48.
[7] Y.H. Xu, D.H. Liang, M.L. Liu, D.Z. Liu, Mater. Res. Bull. 43 (2008) 3474–3482.
[8] O.K. Varghese, M. Paulose, T.J. LaTempa, C.A. Grimes, Nano Lett. 9 (2009) 731–737.
[9] O. Ishitani, C. Inoue, Y. Suzuki, T. Ibusuki, J. Photochem. Photobiol. A-Chem. 72 (1993) 269–271.
[10] M. Anpo, H. Yamashita, K. Ikeue, Y. Fujii, S.G. Zhang, Y. Ichihashi, D.R. Park, Y. Suzuki, K. Koyano, T. Tatsumi, Catal. Today 44 (1998) 327–332.
[11] H. Yamashita, Y. Fujii, Y. Ichihashi, S.G. Zhang, K. Ikeue, D.R. Park, K. Koyano, T. Tatsumi, M. Anpo, Catal. Today 45 (1998) 221–227.
[12] K. Ikeue, S. Nozaki, M. Ogawa, M. Anpo, Catal. Today 74 (2002) 241–248.
[13] Y. Shioya, K. Ikeue, M. Ogawa, M. Anpo, Appl. Catal. A-Gen. 254 (2003) 251–259.
[14] N. Sasirekha, S.J.S. Basha, K. Shanthi, Appl. Catal. B-Environ. 62 (2006) 169–180.
[15] Y. Li, P. Murphy, C.Y. Wu, Fuel Process. Technol. 89 (2008) 567–573.
[16] Y. Li, C.Y. Wu, Environ. Eng. Sci. 24 (2007) 3–12.
[17] I.H. Tseng, J.C.S. Wu, H.Y. Chou, J. Catal. 221 (2004) 432–440.
[18] X.H. Xia, Z.H. Jia, Y. Yu, Y. Liang, Z. Wang, L.L. Ma, Carbon 45 (2007) 717–721.
[19] T.V. Nguyen, J.C.S. Wu, Sol. Energy Mater. Sol. Cells 92 (2008) 864–872.
[20] J.C.S. Wu, H.M. Lin, C.L. Lai, Appl. Catal. A-Gen. 296 (2005) 194–200.
[21] B.F. Xin, P. Wang, D.D. Ding, J. Liu, Z.Y. Ren, H.G. Fu, Appl. Surf. Sci. 254 (2008) 2569–2574.
[22] G. Colon, M. Maicu, M.C. Hidalgo, J.A. Navio, Appl. Catal. B-Environ. 67 (2006) 41–51.
[23] S. Sakthivel, M.C. Hidalgo, D.W. Bahnemann, S.U. Geissen, V. Murugesan, A. Vogelpohl, Appl. Catal. B-Environ. 63 (2006) 31–40.
[24] E.E. Benson, C.P. Kubiak, A.J. Sathrum, J.M. Smieja, Chem. Soc. Rev. 38 (2009) 89–99.
[25] F. Saladin, I. Alxneit, J. Chem. Soc.-Faraday Trans. 93 (1997) 4159–4163.
[26] K.X. Song, J.H. Zhou, J.C. Bao, Y.Y. Feng, J. Am. Ceram. Soc. 91 (2008) 1369–1371.
[27] A. Fujishima, T.N. Rao, D.A. Tryk, J. Photochem. Photobiol. C: Photochem. Rev. 1 (2000) 1–21.